

A Multilevel Active Front-End Rectifier With Current Harmonic Compensation Capability

Franco Hernández⁽¹⁾ Student IEEE Luis Morán⁽¹⁾, Senior IEEE José Espinoza⁽¹⁾, Member IEEE Juan Dixon⁽²⁾, Senior IEEE

⁽¹⁾ Depto. de Ingeniería Eléctrica, Universidad de Concepción, Casilla 160-C. Concepción, CHILE, lmoran@die.udec.cl

⁽²⁾ Depto. de Ingeniería Eléctrica, Universidad Católica, Casilla 306 – Correo 22, Santiago – CHILE, jdixon@ing.puc.cl

Abstract. This paper presents a multilevel active front-end rectifier that can absorb current harmonics generated by nonlinear loads connected to the same power distribution bus. That is, the proposed active front-end converter can operate as an active power filter and simultaneously as a rectifier. The control scheme is simple and forces the power system line current to be sinusoidal and in phase with the respective phase to neutral voltage, and is designed for the application in multilevel rectifiers. The control scheme is described in terms of principles of operations, dynamic modeling, and design. Simulated results are tested for steady state and transient operating conditions on a 10 kVA laboratory prototype.

I. INTRODUCTION

Multilevel active front-end converters have demonstrated to be a viable solution for medium voltage static power conversion [1] – [3]. The series connection of multiples electrolytic capacitors in the dc bus allows the operation in medium voltage systems, presenting lower voltage stresses across each semiconductor [4], in both cases as a rectifier or as multilevel inverter. Moreover, the multi-step composition of the output voltage (for the inverter), or the input current (for the rectifier) presents lower harmonic distortion as compared with the two levels approach, for the same switching frequency, due to the presence of multiple steps in the respective waveforms. The main application of this converter topology has been found in ac drives and also in reactive power compensators.

Active front-end rectifiers (AFE) present near sinusoidal input currents with leading or unity power factor. Another advantage of AFE rectifiers is the regeneration capability, especially for drive applications. One major concern is the voltage distribution across each electrolytic capacitor, which depends on the control scheme, and the associated dynamic response [5]. The operation with unbalanced voltage in the dc bus affects the converter performance due to the generation of uncharacteristic harmonics in the inverter output voltage and rectifier input current and the presence of overvoltages across the semiconductor switches. Significant research has been carried out during the last decade trying to optimize the multilevel converter topology making possible the implementation of a larger number of levels, and the development and implementation of adequate PWM techniques to improve the overall converter performance [6]. Most of this research has been oriented for the specific operation as active front-end rectifiers or as multilevel inverters. Typically, the control scheme of the AFE rectifier has been implemented using the synchronous reference

frame transformation. By controlling i_d and i_q at the rectifier input side, the active and reactive power absorbed by the converter can be changed following the respective reference signals. The control algorithm that uses d-q transformation requires a more complex hardware and software implementation.

The power circuit topology of an active front-end three levels rectifier is shown in Fig. 1. The block diagram of the proposed control scheme is shown in Fig. 2, and the principles of operation are explained with more details in [7].

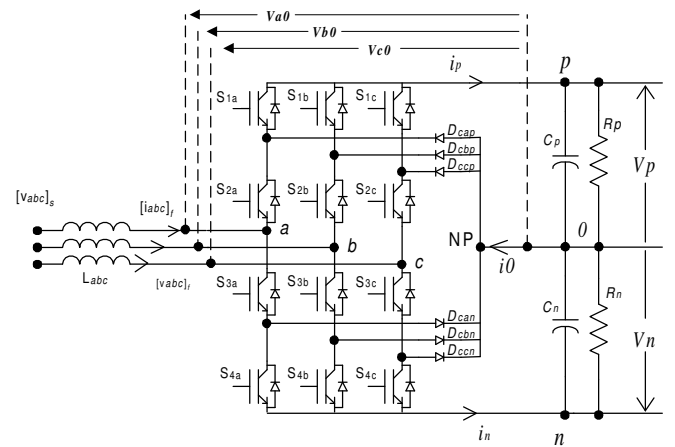


Fig. 1. Power circuit topology of a three-level active front-end rectifier.

Active power filters have been designed to compensate current harmonics, however due to cost restrictions they are not been used in power distribution systems. However, dynamic compensation of reactive power and current harmonics is always required and can be achieved with active front-end rectifiers without the necessity of a converter dedicated only to this task. This is the main advantage of the proposed converter, since it can perform both operations simultaneously, with the extra cost of a larger value of the rectifier rated power required especially for reactive compensation.

In this paper, the proposed active front-end rectifier is discussed in terms of principles of operations for steady-state and transient operating conditions, as a frequency changer and active power filter respectively. The dynamic model of the control scheme is derived allowing the correct tuning of the rectifier controllers. Finally, simulated results are proved on a 10 kVA laboratory prototype.

II. PRINCIPLES OF OPERATION

The most important characteristic of the proposed control scheme is that allows the operation of the active

front-end converter as a rectifier and active power filter simultaneously [7]. This can be achieved since the proposed control scheme performs two important duties. The first one is to keep the converter dc bus voltage constant, balanced across each electrolytic capacitor and equal to a reference, and the second one is to force the power distribution system current to be sinusoidal and in phase with the respective phase-to-neutral voltage, independently of the load impedance connected in the same power distribution bus. The control system block diagram is shown in Fig. 2. It is composed of a current controller and the dc voltage control loop, which keeps the total dc bus voltage constant and equal to a given reference value and a differential voltage controller in charge of keeping the capacitor voltages balanced.

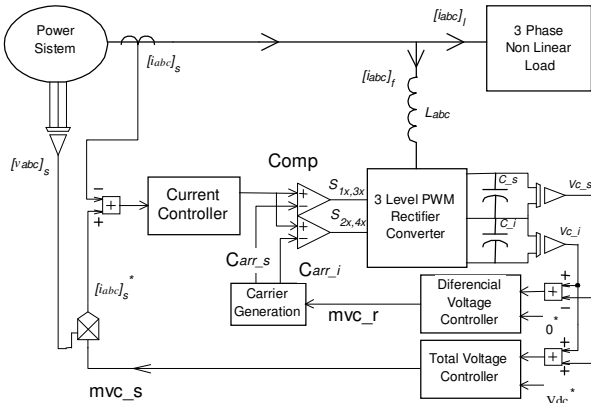


Fig. 2. The block diagram of the proposed control scheme.

By forcing the system line current to be sinusoidal and in phase with the respective phase voltage, the active front-end converter can operate as a rectifier (in case it has a load connected to the dc bus), or as an active filter (in case no load is connected to the dc bus). Another advantage of this control scheme is that does not require to decouple active and reactive power neither to obtain the system current harmonics that need to be eliminated. The three-phase line currents $[i_{abc}]_s$ are forced to follow a reference waveform obtained from one phase to neutral system voltage. The differential voltage controller keeps the same voltage value across each electrolytic capacitor, by adjusting the amplitude of the respective triangular carrier waveform used to generate the gating signals[5]. Simulated results shown in Figs. 3 and 4 illustrate the accurate performance of the control scheme.

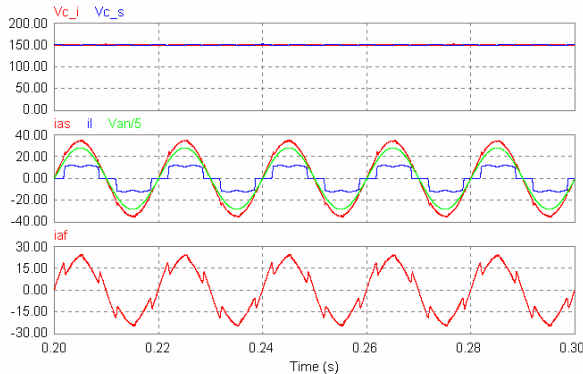


Fig. 3. Active front-end converter operating as a rectifier and active power filter simultaneously, with balanced dc load. (a) Dc voltages across the two electrolytic capacitors. (b) System line current, i_{as} , power system non linear load current, i_i , and ac mains phase to neutral voltage, V_{an} . (c) Active front-end converter input current.

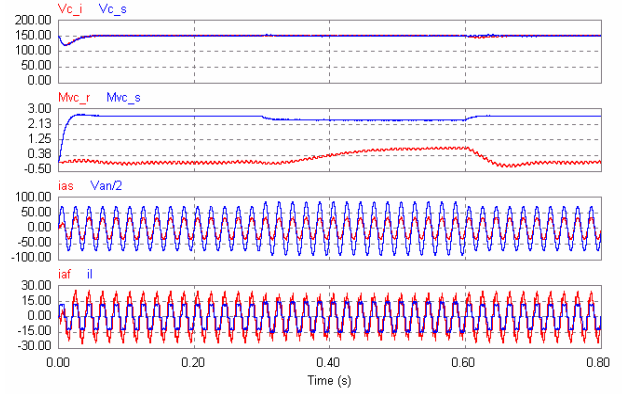


Fig. 4. Transient response of the active front-end converter operating as a rectifier and active power filter simultaneously, with unbalanced dc load. (a) Dc voltages across the two electrolytic capacitors, V_{c_i} and V_{c_s} . (b) Differential voltage controller output signal M_{vc_r} and total voltage controller output signal, M_{vc_s} . (c) System line current, i_{as} , and ac mains phase to neutral voltage, V_{an} . (d) Active front-end converter input current, i_{af} , and nonlinear load current, i_i .

The proposed control scheme is able to balance the distribution system line currents in case single phase or unbalanced load is connected to the same bus, since the reference signal used to generate the converter line current imposes the circulation of balanced current in the distribution bus. Voltage or current unbalance presents in the power distribution system only affects the amplitude of the system line current, which is automatically adjusted so the power required by the converter and other loads is not changed. Figure 5 shows the system current and voltage waveforms when one of the nonlinear load phases opens. In this case the phase load current, i_{ia} , goes to zero (Fig. 5-d), but the system currents remains balanced and with unity power factor (Fig. 5-c). That means that the converter control scheme is able to distribute the phase power in the power distribution three phases, forcing the proposed active front-end converter and unbalanced non linear load to behave as a pure resistive and balanced equivalent load.

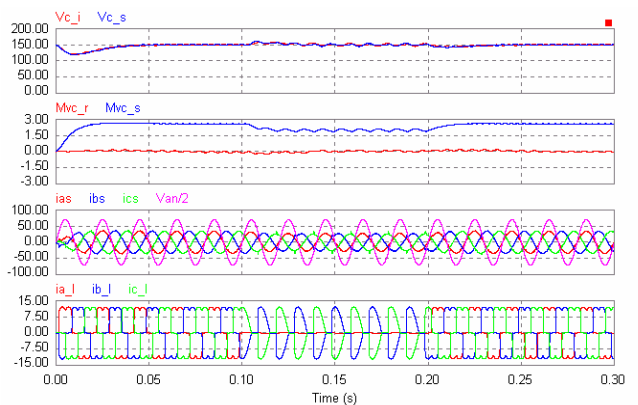


Fig. 5. Active front-end converter operating as a rectifier and active power filter simultaneously, with unbalance system load current (Phase a of the load is open between 0.1 and 0.2 s). (a) Dc voltages across the two electrolytic capacitors, V_{c_i} and V_{c_s} . (b) Differential voltage controller output signal M_{vc_r} and total voltage controller output signal, M_{vc_s} . (c) System three phase line currents, i_{as} , i_{bs} , i_{cs} , and ac mains phase to neutral voltage, V_{an} . (d) Three phase non linear load currents, i_{a_l} , i_{b_l} , i_{c_l} .

III. CONVERTER DYNAMICAL MODEL

The converter mathematical model is derived from the gating signals generator system (switching functions), and

relates the rectifier input currents with the dc bus voltage. The derived model allows the design of the control that keeps the dc voltage constant and balanced, and helps to find the converter stability region for different operating condition.

A. Converter Mathematical Model

The positive and negative current that flows through the rectifier dc bus are defined by the following equations:

$$i_p = S_{ap} \cdot i_a + S_{bp} \cdot i_b + S_{cp} \cdot i_c \quad (1)$$

$$i_n = S_{an} \cdot i_a + S_{bn} \cdot i_b + S_{cn} \cdot i_c \quad (2)$$

where S_{ap} , S_{bp} , S_{cp} , S_{an} , S_{bn} , and S_{cn} are the rectifier switching functions for the positive (e.g. S_{1a} , S_{2a}) and negative (e.g. S_{3a} , S_{4a}) switches. The relation between the rectifier input line voltages and the voltages across each electrolytic capacitor are defined by:

$$\begin{bmatrix} v_{ab} \\ v_{bc} \\ v_{ca} \end{bmatrix} = \begin{bmatrix} S_{abp} & S_{abn} \\ S_{bcp} & S_{bcn} \\ S_{cap} & S_{can} \end{bmatrix} \cdot \begin{pmatrix} V_p \\ V_n \end{pmatrix} \quad (3)$$

From Fig. 1 the following relations are derived:

$$V_p - V_n = v_{dc} \quad (4)$$

$$V_p + V_n = 2 \cdot \Delta v_{dc} \quad (5)$$

Replacing (4) and (5) in (3):

$$\begin{bmatrix} v_{ab} \\ v_{bc} \\ v_{ca} \end{bmatrix} = \begin{bmatrix} S_{abp} - S_{abn} \\ S_{bcp} - S_{bcn} \\ S_{cap} - S_{can} \end{bmatrix} \cdot \frac{v_{dc}}{2} + \begin{bmatrix} S_{abp} + S_{abn} \\ S_{bcp} + S_{bcn} \\ S_{cap} + S_{can} \end{bmatrix} \cdot \Delta v_{dc} \quad (6)$$

Also, from Fig. 1:

$$i_n = C_n \frac{dV_n}{dt} + \frac{V_n}{R_n} \quad (7)$$

$$i_p = C_p \frac{dV_p}{dt} + \frac{V_p}{R_p} \quad (8)$$

but $C_n = C_p = C$ and the neutral current, i_o , is equal to $i_n + i_p$. The equations that relate the system line voltages with the converter input currents and dc voltages are:

$$\begin{bmatrix} v_{abs} \\ v_{bcs} \\ v_{cas} \end{bmatrix} = L \cdot \begin{bmatrix} d(i_a - i_b)/dt \\ d(i_b - i_c)/dt \\ d(i_c - i_a)/dt \end{bmatrix} + \begin{bmatrix} v_{ab} \\ v_{bc} \\ v_{ca} \end{bmatrix} \quad (9)$$

By replacing (9) in (6) the final sets of equations that represent the dynamical model of the front-end rectifier in abc reference frame are obtained.

$$\frac{d(i_{sn})}{dt} = \frac{1}{3L} \cdot v_s - \frac{1}{3L} S \frac{v_{dc}}{2} - \frac{1}{3L} S_{np} \Delta v_{dc} \quad (10)$$

$$\frac{d(v_{dc})}{dt} = \frac{1}{C} S^T \cdot i_{sn} - \frac{v_{dc}}{2C} \left(\frac{1}{R_p} + \frac{1}{R_n} \right) - \Delta v_{dc} \quad (11)$$

$$\frac{d(\Delta v_{dc})}{dt} = \frac{1}{2C} S_{np}^T \cdot i_{sn} + \frac{v_{dc}}{4C} \left(\frac{1}{R_n} - \frac{1}{R_p} \right) - \frac{\Delta v_{dc}}{2C} \left(\frac{1}{R_p} + \frac{1}{R_n} \right) \quad (12)$$

The switching function matrices S and S_{np} are derived from the gating signals generator block that contains the sinusoidal reference signal and the two triangular carrier waveforms, as shown in Fig. 6. The derivation of the two switching functions is obtained from the intersection of the two signals.

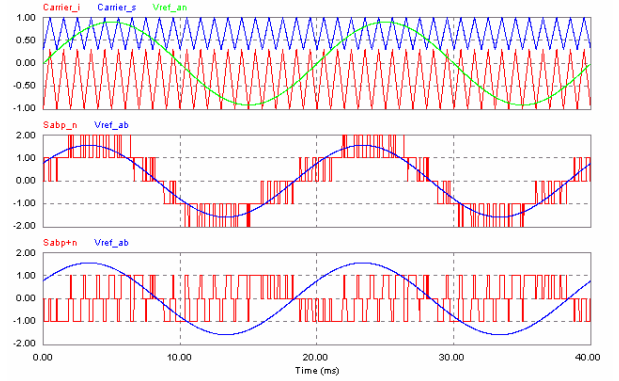


Fig. 6. Line to line switching functions for the three-level active front-end rectifier, S_{ab} and S_{np} . (a) Sinusoidal reference waveform, V_{ref_an} , and triangular carrier waveforms, $Carrier_s$ and $Carrier_i$. (b) Rectifier line to line switching function S . (c) Rectifier line to neutral switching function S_{np} .

The active front-end rectifier operates with two switching functions: S which defines the rectifier input voltage waveform, and S_{np} which is the one that has the information regarding the voltage unbalanced across the electrolytic capacitors. The mathematical functions that represent S_{ap} and S_{an} have the following expression:

$$S_{ap}(t) = m \cdot \sin(\omega t) - d \quad (13)$$

$$S_{an}(t) = d - m \cdot \sin(\omega t) \quad (14)$$

where m is the rectifier modulation index and d the unbalanced factor across the two electrolytic capacitors (Fig. 6). By using Fourier series, the expressions that define the rectifier switching functions S_{ap} , S_{bp} and S_{cp} are the followings:

$$\begin{aligned} S_{ap} &= \left\{ \frac{1}{(1-d)} \left[\frac{m}{2} - \frac{m}{\pi} \sin^{-1}\left(\frac{d}{m}\right) - \frac{d}{\pi} \cos\left(\sin^{-1}\left(\frac{d}{m}\right)\right) \right] \right\} \sin(\omega t) \\ S_{bp} &= \left\{ \frac{1}{(1-d)} \left[\frac{m}{2} - \frac{m}{\pi} \sin^{-1}\left(\frac{d}{m}\right) - \frac{d}{\pi} \cos\left(\sin^{-1}\left(\frac{d}{m}\right)\right) \right] \right\} \sin\left(\omega t - \frac{2\pi}{3}\right) \\ S_{cp} &= \left\{ \frac{1}{(1-d)} \left[\frac{m}{2} - \frac{m}{\pi} \sin^{-1}\left(\frac{d}{m}\right) - \frac{d}{\pi} \cos\left(\sin^{-1}\left(\frac{d}{m}\right)\right) \right] \right\} \sin\left(\omega t + \frac{2\pi}{3}\right) \end{aligned} \quad (15)$$

Following the same procedure to obtain S_{an} , S_{bn} , and S_{cn} :

$$\begin{aligned} S_{an} &= \frac{1}{1+d} \left[-\frac{m}{2} - \frac{m}{\pi} \sin^{-1}\left(\frac{d}{m}\right) - \frac{d}{\pi} \cos\left(\sin^{-1}\left(\frac{d}{m}\right)\right) \right] \sin(\omega t) \\ S_{bn} &= \frac{1}{1+d} \left[-\frac{m}{2} - \frac{m}{\pi} \sin^{-1}\left(\frac{d}{m}\right) - \frac{d}{\pi} \cos\left(\sin^{-1}\left(\frac{d}{m}\right)\right) \right] \sin\left(\omega t - \frac{2\pi}{3}\right) \\ S_{cn} &= \frac{1}{1+d} \left[-\frac{m}{2} - \frac{m}{\pi} \sin^{-1}\left(\frac{d}{m}\right) - \frac{d}{\pi} \cos\left(\sin^{-1}\left(\frac{d}{m}\right)\right) \right] \sin\left(\omega t + \frac{2\pi}{3}\right) \end{aligned} \quad (16)$$

Since:

$$S = \begin{bmatrix} S_{abp} - S_{abn} \\ S_{bcp} - S_{bcn} \\ S_{cap} - S_{can} \end{bmatrix} \text{ and } \begin{bmatrix} S_{abp,n} = S_{ap,n} - S_{bp,n} \\ S_{bcp,n} = S_{bp,n} - S_{cp,n} \\ S_{cap,n} = S_{cp,n} - S_{ap,n} \end{bmatrix} \quad (17)$$

Finally:

$$S = \frac{\sqrt{3}}{(1-d^2)} \begin{bmatrix} m - \frac{2dm}{\pi} \sin^{-1}\left(\frac{d}{m}\right) - \frac{2d^2}{\pi} \cos\left(\sin^{-1}\left(\frac{d}{m}\right)\right) \sin\left(\omega t + \frac{\pi}{6}\right) \\ m - \frac{2dm}{\pi} \sin^{-1}\left(\frac{d}{m}\right) - \frac{2d^2}{\pi} \cos\left(\sin^{-1}\left(\frac{d}{m}\right)\right) \sin\left(\omega t - \frac{\pi}{2}\right) \\ m - \frac{2dm}{\pi} \sin^{-1}\left(\frac{d}{m}\right) - \frac{2d^2}{\pi} \cos\left(\sin^{-1}\left(\frac{d}{m}\right)\right) \sin\left(\omega t + \frac{5\pi}{6}\right) \end{bmatrix} \quad (18)$$

The transfer switching matrix S_{np} is defined by:

$$S_{np} = \begin{bmatrix} S_{abp} + S_{abn} \\ S_{bcp} + S_{bcn} \\ S_{cap} + S_{can} \end{bmatrix} \quad (19)$$

$$S_{np} = \frac{\sqrt{3}}{(1-d^2)} \begin{bmatrix} dm - \frac{2m}{\pi} \sin^{-1}\left(\frac{d}{m}\right) - \frac{2d}{\pi} \cos\left(\sin^{-1}\left(\frac{d}{m}\right)\right) \sin\left(\omega t + \frac{\pi}{6}\right) \\ dm - \frac{2m}{\pi} \sin^{-1}\left(\frac{d}{m}\right) - \frac{2d}{\pi} \cos\left(\sin^{-1}\left(\frac{d}{m}\right)\right) \sin\left(\omega t - \frac{\pi}{2}\right) \\ dm - \frac{2m}{\pi} \sin^{-1}\left(\frac{d}{m}\right) - \frac{2d}{\pi} \cos\left(\sin^{-1}\left(\frac{d}{m}\right)\right) \sin\left(\omega t + \frac{5\pi}{6}\right) \end{bmatrix}$$

The set of equations (10), (11) and (12) can be simplified by using the Park Transformation. In the dq reference frame the converter equations are the following:

$$\begin{aligned} \frac{d[i_{sn}]_{dq}}{dt} + W[i_{sn}]_{dq} &= \frac{1}{3L}[v_s]_{dq} - \frac{1}{6L}[S]_{dq}v_{dc} - \frac{1}{3L}[S_{np}]_{dq}\Delta v_{dc} \\ \frac{d}{dt}(v_{dc}) &= \frac{1}{C}S_{dq}^T[i_{sn}]_{dq} - \frac{v_{dc}}{2C}\left(\frac{R_p + R_n}{R_p R_n}\right) - \frac{\Delta v_{dc}}{C}\left(\frac{R_n - R_p}{R_p R_n}\right) \\ \frac{d(\Delta v_{dc})}{dt} &= \frac{1}{2C}[S_{np}]_{dq}^T[i_{sn}]_{dq} + \frac{v_{dc}}{4C}\left(\frac{R_p - R_n}{R_p R_n}\right) - \frac{\Delta v_{dc}}{2C}\left(\frac{R_p + R_n}{R_p R_n}\right) \end{aligned} \quad (20)$$

$$\text{with } W = \begin{bmatrix} 0 & -\omega \\ \omega & 0 \end{bmatrix} \text{ and } \omega = 2\pi f.$$

B. Converter Operating Region

The converter operating region defined by a set of values i_{snd} , i_{snq} , v_{dc} , and Δv_{dc} , that keeps the converter in a stable operating condition is obtained from the solution of the following equations:

$$\begin{aligned} \omega i_{snq} + \frac{v_{sd}}{3L} - \frac{S_d}{6L}v_{dc} - \frac{S_{np}}{3L}\Delta v_{dc} &= 0 \\ -\omega i_{snd} + \frac{v_{sq}}{3L} - \frac{S_q}{6L}v_{dc} - \frac{S_{np}}{3L}\Delta v_{dc} &= 0 \\ \frac{1}{C}(S_d i_{snd} + S_q i_{snq}) - \frac{v_{dc}}{2C}\left(\frac{R_p + R_n}{R_p R_n}\right) - \frac{\Delta v_{dc}}{C}\left(\frac{R_n + R_p}{R_n R_p}\right) &= 0 \\ \frac{1}{2C}(S_{npd} i_{snd} + S_{npq} i_{snq}) + \frac{v_{dc}}{4C}\left(\frac{R_p - R_n}{R_p R_n}\right) - \frac{\Delta v_{dc}}{2C}\left(\frac{R_p + R_n}{R_p R_n}\right) &= 0 \end{aligned} \quad (21)$$

The converter operating point associated with the values selected for the implementation of the converter laboratory prototype are:

$$\begin{aligned} d &= 0 & i_{snq} &= 0 & V_{dc} &= 300 \text{ V} \\ R &= R_n = R_p = 10 \text{ } \Omega & L &= 3 \text{ mH} \\ S_{npd} &= 0 & S_{npq} &= 0 \end{aligned}$$

Also:

$$S_d = \sqrt{\frac{3}{2}} \cdot f_1(m, d) \cos(\alpha) \quad S_q = \sqrt{\frac{3}{2}} \cdot f_1(m, d) \sin(\alpha)$$

The converter applied voltages in d, q frame are $v_{sd} = 300 \text{ V}$ and $v_{sq} = 0 \text{ V}$. By replacing these values in (21), the following equations must be solved.

$$\begin{aligned} 2v_{sd} - \sqrt{\frac{3}{2}} f_1(m, 0) \cdot \cos(\alpha) \cdot v_{dc} &= 0 \\ -6L\omega i_{snd} - \sqrt{\frac{3}{2}} f_1(m, 0) \cdot \sin(\alpha) \cdot v_{dc} &= 0 \end{aligned}$$

$$\sqrt{\frac{3}{2}} R f_1(m, 0) \cdot \cos(\alpha) \cdot i_{snd} - v_{dc} = 0$$

The two possible solutions are:

$$\begin{bmatrix} f_1 \\ \alpha \\ i_{snd} \end{bmatrix} = \begin{bmatrix} -1.6992 & 1.6492 \\ 3.001 & -0.1404 \\ -15.00 & 15.00 \end{bmatrix}$$

The final solution is $(f_1, \alpha, i_{snd}) = (1.6492, -0.1404, 15.00)$. That means converter modulation index $m = 0.95$, switching function phase shift angle, $\alpha = -8.05^\circ$, rectifier input current $i_a = 15 \text{ A}$.

C. Converter Linearized Control Model

The system model (20) can be linearized around a given operating point as shown in (22).

$$\begin{aligned} \begin{bmatrix} \delta i_{sn_d} \\ \delta i_{sn_q} \\ \delta v_{dc} \\ \delta \Delta v_{dc} \end{bmatrix} &= \begin{bmatrix} 0 & w & -\frac{\sqrt{18}m}{12L} \cos(\alpha) & 0 \\ -w & 0 & -\frac{\sqrt{18}m}{12L} \sin(\alpha) & 0 \\ \frac{\sqrt{18} \cdot m}{2C} \cos(\alpha) & \frac{\sqrt{18} \cdot m}{2C} \sin(\alpha) & -\frac{(R_p + R_n)}{2CR_p R_n} & 0 \\ 0 & 0 & 0 & -\frac{(R_p + R_n)}{2CR_p R_n} \end{bmatrix} \begin{bmatrix} \delta i_{sn_d} \\ \delta i_{sn_q} \\ \delta v_{dc} \\ \delta \Delta v_{dc} \end{bmatrix} \\ &+ \begin{bmatrix} -\frac{\sqrt{18}}{12L} \cos(\alpha) v_{dc} & 0 & \frac{\sqrt{18}m}{12L} \sin(\alpha) v_{dc} \\ -\frac{\sqrt{18}}{12L} \sin(\alpha) v_{dc} & 0 & -\frac{\sqrt{18}m}{12L} \cos(\alpha) v_{dc} \\ \frac{\sqrt{18}}{2C} \cos(\alpha) i_{sn_d} & 0 & \frac{\sqrt{18}m}{2C} \sin(\alpha) i_{snd} \\ 0 & \frac{\sqrt{18} \left(m - \frac{4}{\pi}\right)}{4C} \cos(\alpha) i_{sn_d} & 0 \end{bmatrix} \begin{bmatrix} \delta m \\ \delta \alpha \\ \delta i_{snd} \end{bmatrix} + \begin{bmatrix} \frac{1}{3L} & 0 \\ 0 & \frac{1}{3L} \\ 0 & 0 \\ 0 & 0 \end{bmatrix} \begin{bmatrix} \delta v_{s_d} \\ \delta v_{s_q} \end{bmatrix} \end{aligned} \quad (22)$$

The block diagram of the converter control scheme is shown in Fig. 7. The controller time constant can be derived from the following equations:

Current Controller:

$$\frac{\delta m(s)}{\delta i_{snq}^*(s) - K_i \delta i_{snq}(s)} = \frac{\delta \alpha(s)}{\delta i_{snd}^*(s) - K_i \delta i_{snd}(s)} = \left[K_{pi} + \frac{1}{T_{ii} \cdot s} \right]$$

Differential Voltage Controller:

$$\frac{\delta d(s)}{\delta \Delta v_{dc}^*(s) - K_{vdc} \delta v_{dc}} = \left[K_{p\Delta} + \frac{1}{T_{i\Delta} \cdot s} \right]$$

Dc bus Voltage Controller:

$$\frac{i_{snd}^*(s)}{\delta v_{dc}^*(s) - K_{vdc} \cdot \delta v_{dc}} = \left[K_{pT} + \frac{1}{T_{iT} \cdot s} \right]$$

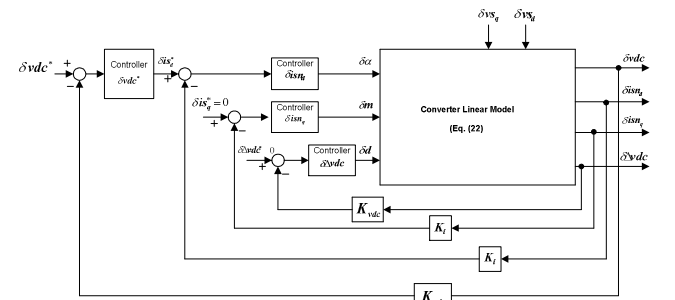


Fig. 7. Converter control scheme block diagram.

IV. EXPERIMENTAL RESULTS

The mathematical model and simulated results were tested in a 10 kVA laboratory prototype. Experimental waveforms shown in the following figures prove the validity of the model, the developed control scheme and simulated results.

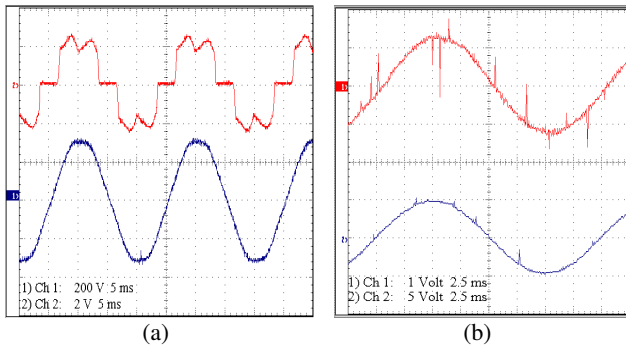


Fig. 8. Active front-end converter operating as an active power filter. (a) Nonlinear load current (12.5 A/div) and system phase to neutral voltage (100 V/div). (b) Power system line current (5 A/div) and phase to neutral system voltage (200 V/div).

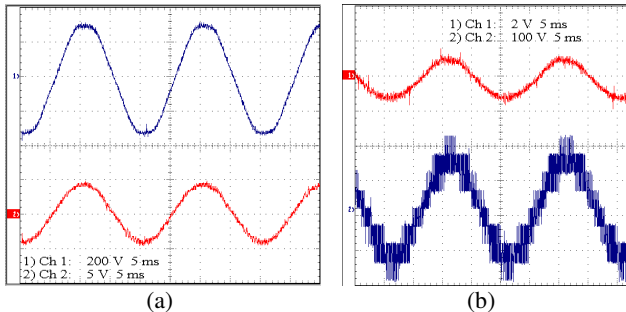


Fig. 9. Active front-end converter operating as a rectifier with unity power factor. (a) Phase to neutral system voltage (200 V/div) and rectifier input current (12.5 A/div). (b) System line current (5 A/div) and rectifier input line to line voltage (100 V/div).

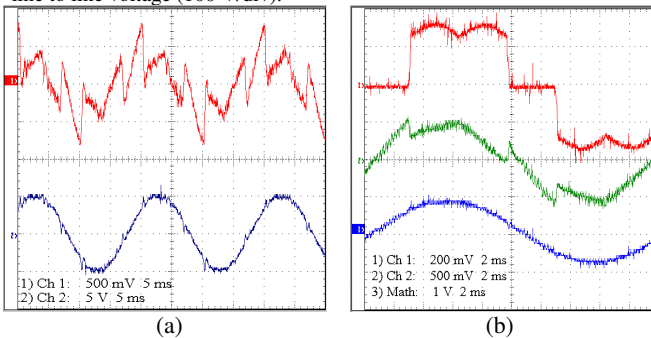


Fig. 10. Active front-end converter operating as a rectifier and active power filter simultaneously. (a) Active front-end input current (100mV/A) and system line current (12.5 A/div). (b) Nonlinear load current (100 mV/A), active front-end converter input current (100 mV/A), system line current (100 mv/A).

Figures 8, 9 and 10 show the effectiveness of the active front-end converter in absorbing current harmonics generated by the non linear load. The system line current is sinusoidal and in phase with the respective phase to neutral voltage, as shown in Fig. 8. Figure 10 shows that the converter input current is distorted when it is connected in conjunction with a nonlinear load.

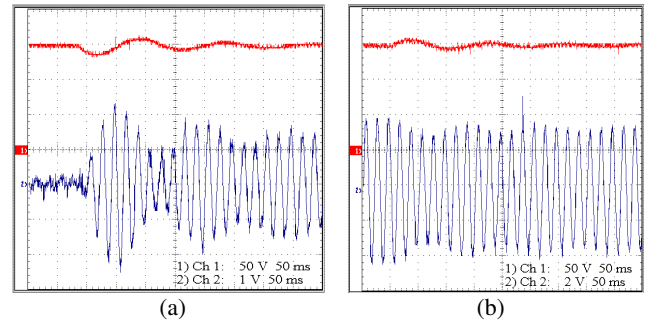


Fig. 11. Active front-end converter transient response for operation as active power filter. (a) Upper capacitor dc voltage (50 V/div) and system line current (2.5 A/div) for a step increment in the nonlinear load. (b) Upper capacitor dc voltage (50 V/div) and system line current (5 A/div) for a step reduction in the nonlinear load.

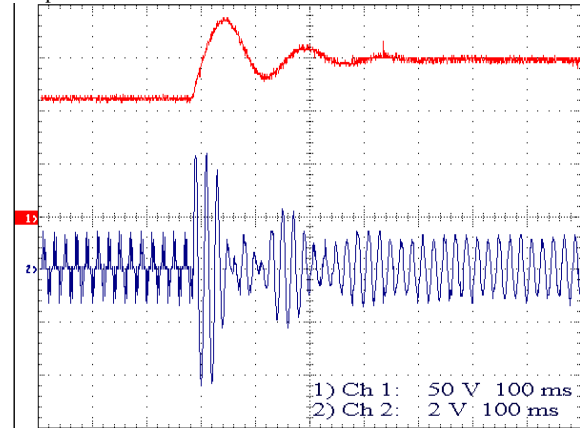


Fig. 12. Active front-end converter for operation as active power filter, instant at which controllers start to operate. (a) Upper capacitor dc voltage (50 V/div). (b) System line current (5 A/div).

Transient responses of the converter are shown in Figs. 11, 12 and 13. The dc bus voltage is stabilized after a change is generated in the load, or after the controller start to operate. Also, the differential dc voltage controller equalizes the two voltages in 250 ms, showing the expected time response.

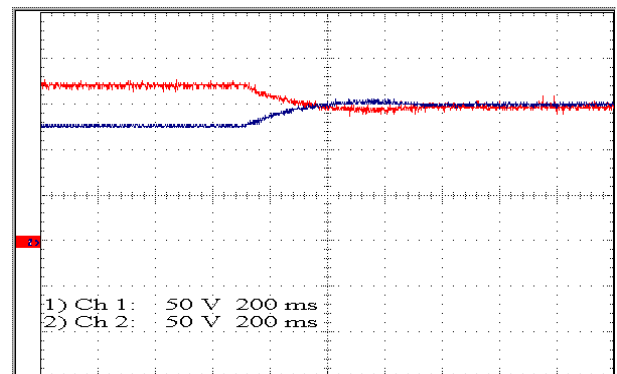


Fig. 13. Transient response of the converter differential voltage controller. (a) Voltage across the top and bottom electrolytic capacitors, v_{es} (50 V/div) and v_{ei} (50 V/div).

ACKNOWLEDGMENT

The authors would like to thanks Fondecyt (the Chilean Research Council) for the financial support given through the project # 1020460.

V. CONCLUSION

A control scheme that allows the operation of a three level active front-end converter as a rectifier, active power filter and both at the same time has been presented. The proposed control scheme is very robust since allows the operation of the active front-end converter under unbalanced input voltage conditions. The control scheme forces the power distribution line current to be sinusoidal and in phase with the respective phase to neutral voltage, and keeps the total dc voltage constant and balanced across each electrolytic capacitor. The close agreement between simulated results and a 10 kVA laboratory prototype proves the validity of the developed scheme.

VI. REFERENCES

- [1] J. S. Lai and F. Z. Peng, "Multilevel Converters A New Breed of Power Converters," in *IEEE Trans. Ind. Applic.*, vol. IA-32, N° 3, May/June 1996, pp. 509-517.
- [2] G. Walker and G. Ledwich, "Bandwidth Considerations for Multilevel Converters," in *IEEE Trans. on Power Electronics*, Vol. 14, N° 1, January 1999, pp. 74-81.
- [3] A. Nabae, I. Takahashi, and H. Akagi, "A New Neutral-Point-Clamped PWM Inverter," in *IEEE Trans. on Ind. Applic.* Vol. IA-17, N° 5, Sep./Oct. 1981, pp. 518-523.
- [4] R. Rojas, T. Ohnishi, and T. Suzuki, "An Improved Voltage Vector Control Method for Neutral-Point-Clamped Inverters," in *IEEE Trans. on Power Electronics*, Vol. 10, N° 6, Nov. 1995, pp. 666-672.
- [5] N. Celanovic and D. Boroyevich, "A Comprehensive Study of Neutral-Point Voltage Balancing Problems in Three-Level Neutral-Point-Clamped Voltage Source Inverters" in *IEEE Trans. on Power Electronics*, Vol. 15, N° 2, March 2000, pp. 242-249.
- [6] M. Liserre, A. Dell'Aquila, F. Blaabjerg, "Design and Control of a Three-Phase Active Rectifier Under Non-Ideal Operating Conditions," in *IEEE IAS Annual Meeting Proceedings*, Pittsburgh, October 2002, (in CD version).
- [7] F. Hernández, L. Morán, J. Espinoza, J. Dixon, "A Generalized Control Scheme for Active Front-end Multilevel Converters," in *IEEE Industrial Electronics Conference*, Denver, November 2002, (in CD version).

